JCI insight

RESEARCH ARTICLE

Adipocyte JAK2 mediates spontaneous metabolic liver disease and hepatocellular carcinoma

Kevin C. Corbit,[1] Camella G. Wilson,[1] Dylan Lowe,[1] Jennifer L. Tran,[1] Nicholas B. Vera,[2] Michelle Clasquin,[2] Aras N. Mattis,[3] and Ethan J. Weiss[1]

[1]Cardiovascular Research Institute, UCSF, San Francisco, California, USA. [2]Cambridge Laboratories, Pfizer Global Research and Development, Pfizer Inc., Cambridge, Massachusetts, USA. [3]Department of Pathology, UCSF, San Francisco, California, USA.

Nonalcoholic fatty liver disease (NAFLD) and steatohepatitis (NASH) are liver manifestations of the metabolic syndrome and can progress to hepatocellular carcinoma (HCC). Loss of growth hormone (GH) signaling is reported to predispose to NAFLD and NASH through direct actions on the liver. Here, we report that aged mice lacking hepatocyte *Jak2* (JAK2L), an obligate transducer of GH signaling, spontaneously develop the full spectrum of phenotypes found in patients with metabolic liver disease, beginning with insulin resistance and lipodystrophy and manifesting as NAFLD, NASH, and even HCC, independent of dietary intervention. Remarkably, insulin resistance, metabolic liver disease, and carcinogenesis are prevented in JAK2L mice via concomitant deletion of adipocyte *Jak2*. Further, we demonstrate that GH increases hepatic lipid burden but does so indirectly via signaling through adipocyte JAK2. Collectively, these data establish adipocytes as the mediator of GH-induced metabolic liver disease and carcinogenesis. In addition, we report what we believe to be a new spontaneous model of NAFLD, NASH, and HCC that recapitulates the natural sequelae of human insulin resistance–associated disease progression. The work presented here suggests that attention be paid to inhibition of adipocyte GH signaling as a therapeutic target of metabolic liver disease.

Introduction

The global prevalence of nonalcoholic fatty liver disease (NAFLD), a state of excess liver lipid accumulation in the absence of chronic alcohol intake, is estimated to be approximately 24% (1). A subset of patients with NAFLD go on to develop non-alcoholic steatohepatitis (NASH) with associated inflammation and fibrosis. NASH is now the leading cause of liver transplantation in the United States and predisposes to hepatocellular carcinoma (HCC) (2), the most common malignancy of the liver worldwide (3). Currently, there are no FDA-approved treatments for NASH, which could be a reflection of the lack of faithful animal models that fully recapitulate its clinical presentation (4, 5).

NASH pathogenesis is complex and multifactorial, though the risk factors are nearly identical to those predisposing to the metabolic syndrome (4). It was revealed nearly 2 decades ago that NAFLD is significantly associated with insulin resistance (IR) (6), and NAFLD-associated hepatic IR is independent of adiposity and glucose intolerance (7). Although the association of IR with fatty liver is strong, the cause-and-effect relationship is unclear. Hepatic fat content results from a balance of fatty acid influx, de novo lipogenesis (DNL), secretion of triglycerides, and catabolism of fatty acids by β-oxidation (8). Given that these 4 processes occur within the liver itself, the majority of research and treatment paradigms for NAFLD, NASH, and HCC have been focused on liver-intrinsic mechanisms.

How IR promotes hepatic lipid accumulation is debated. Insulin suppresses gluconeogenesis and induces DNL in the liver (9). Thus, the predicted consequence of IR is increased glucose production and reduced lipogenesis. However, it is well recognized that the former and not latter pathways are affected in people with diabetes, as high levels of gluconeogenesis coexist with increased hepatic lipid burden in the setting of IR. This phenomenon has been termed "selective IR" and been attributed to both liver-intrinsic and -extrinsic mechanisms (10, 11).

Conflict of interest: NBV and MC are employees and shareholders of Pfizer Inc.

Submitted: June 25, 2019
Accepted: July 30, 2019
Published: September 5, 2019.

Reference information: *JCI Insight*. 2019;4(17):e131310. https://doi.org/10.1172/jci.insight.131310.

Prolonged fasting/starvation, such as in anorexia nervosa (AN), and lipodystrophy (LD) are other conditions associated with fatty liver (12, 13). Interestingly, these states of adipose tissue dysfunction have IR as a commonality and, especially in the case of LD, have biochemical features more closely aligned with prevalent forms of IR than those caused by defects in insulin signaling itself (13). This suggests that adipose tissue dysfunction may be a common feature, and possibly a driver, of various forms of IR.

As is the case with protracted fasting, NAFLD and NASH are associated with adipose tissue dysfunction (13, 14). Growth hormone (GH) is a starvation-induced hormone that controls hepatic and circulating insulin-like growth factor 1 (IGF1) levels and adipose tissue lipolysis during fasting (15, 16) and is elevated in patients with LD (17). Malnutrition, LD, AN, and NAFLD are associated with hepatic GH resistance, which may seem paradoxical, but in fact hepatic GH resistance leads to elevated circulating GH, via loss of IGF1-mediated feedback inhibition, which can act on non-liver, GH-responsive tissues. In fact, treatment of AN patients with GH fails to increase IGF1 levels, confirming hepatic GH resistance, but does further decrease fat mass, indicating that adipose tissue remains GH responsive in the clinically "GH-resistant" state (18). Thus, elevated GH activity on adipose tissue may be a commonality among GH-resistant and IR states, including starvation, LD, and NAFLD/NASH.

GH is a major regulator of glucose and lipid metabolism (19, 20). Congenital loss of global GH signaling increases insulin sensitivity and adiposity and may decrease the incidence of diabetes and cancer (21, 22). Conversely, exposure to GH acutely (19) or chronically, in the setting of acromegaly, induces IR (23). Somewhat paradoxically, adult-onset GH deficiency also predisposes to fatty liver and NASH (24), possibly by a different mechanism via direct effects on hepatic DNL (25). However, a unifying model of how GH impinges on insulin sensitivity to mediate glucose and lipid metabolism has not been universally accepted.

We previously reported that mice with hepatic GH resistance, via hepatocyte-specific deletion of *Jak2* (JAK2L), developed fatty liver in a GH-dependent manner and had early signs of NASH by 20 weeks of age (26). Here, we report that aged JAK2L mice are insulin resistant and lipodystrophic and subsequently develop severe NASH and HCC. These phenotypes recapitulate the features of metabolic liver disease and are entirely dependent on adipocyte JAK2 because mice lacking both hepatocyte and adipocyte *Jak2* (JAK2LA) retained insulin sensitivity and maintained liver homeostasis. Treatment with recombinant GH increased liver triacylglycerol (TAG) and diacylglycerol (DAG) levels in controls but not in mice lacking adipocyte *Jak2* only. Collectively, we demonstrate that adipocytes are the target of GH-induced changes in liver metabolism. Further, we provide a potentially new model of metabolic liver disease that is independent of dietary intervention.

Results

Hepatic GH resistance promotes age-associated IR via adipocyte signaling. We aged cohorts of control (CON, n = 16), JAK2L (n = 14), and JAK2LA (n = 17) mice to between 70 and 75 weeks of age and determined glucose homeostasis in the fed and fasted states. Similar to our previous results in younger mice (27), induction of hepatic GH resistance through hepatocyte-specific deletion of *Jak2* in JAK2L and JAK2LA mice essentially eliminated detectable circulating IGF1 (Figure 1A). This abolished IGF1-mediated negative feedback on central GH production and resulted in approximately 200 times higher fasting serum GH levels in both JAK2L and JAK2LA animals compared with the CON cohort (Figure 1B). Blood glucose levels varied little among the 3 genotypes, with only JAK2LA mice having statistically lower levels of fed glucose compared with CON mice (Figure 1C). CON mice appropriately showed lower serum insulin levels following an overnight fast; however, JAK2L animals had both fed and fasting hyperinsulinemia (Figure 1D). This led to a large increase in the homeostatic assessment model of insulin resistance (HOMA-IR) in the JAK2L mice that was normalized in JAK2LA animals (Figure 1E). Insulin tolerance testing (ITT) revealed augmented responsiveness in JAK2LA mice as compared with CON and JAK2L cohorts (Figure 1F). Although HOMA-IR and ITT results were not concordant in these cohorts, HOMA-IR is more closely correlated with hepatic than peripheral insulin sensitivity (28), consistent with our previous published work using hyperinsulinemic-euglycemic clamps in JAK2L mice (20). Therefore, aged mice lacking hepatocyte *Jak2* are GH resistant and develop IR in an adipocyte *Jak2*–dependent manner.

JAK2L mice are lipodystrophic and have defective adipose tissue signaling in response to feeding. Aged JAK2L mice weighed less than the CON and JAK2LA cohorts in both the fed and fasted states (Figure 2A). Interestingly, JAK2L mice lost more weight following an overnight fast, consistent with the role of GH as a catabolic "starvation" hormone (Figure 2B). Dual-energy x-ray absorptiometry scanning revealed an increase

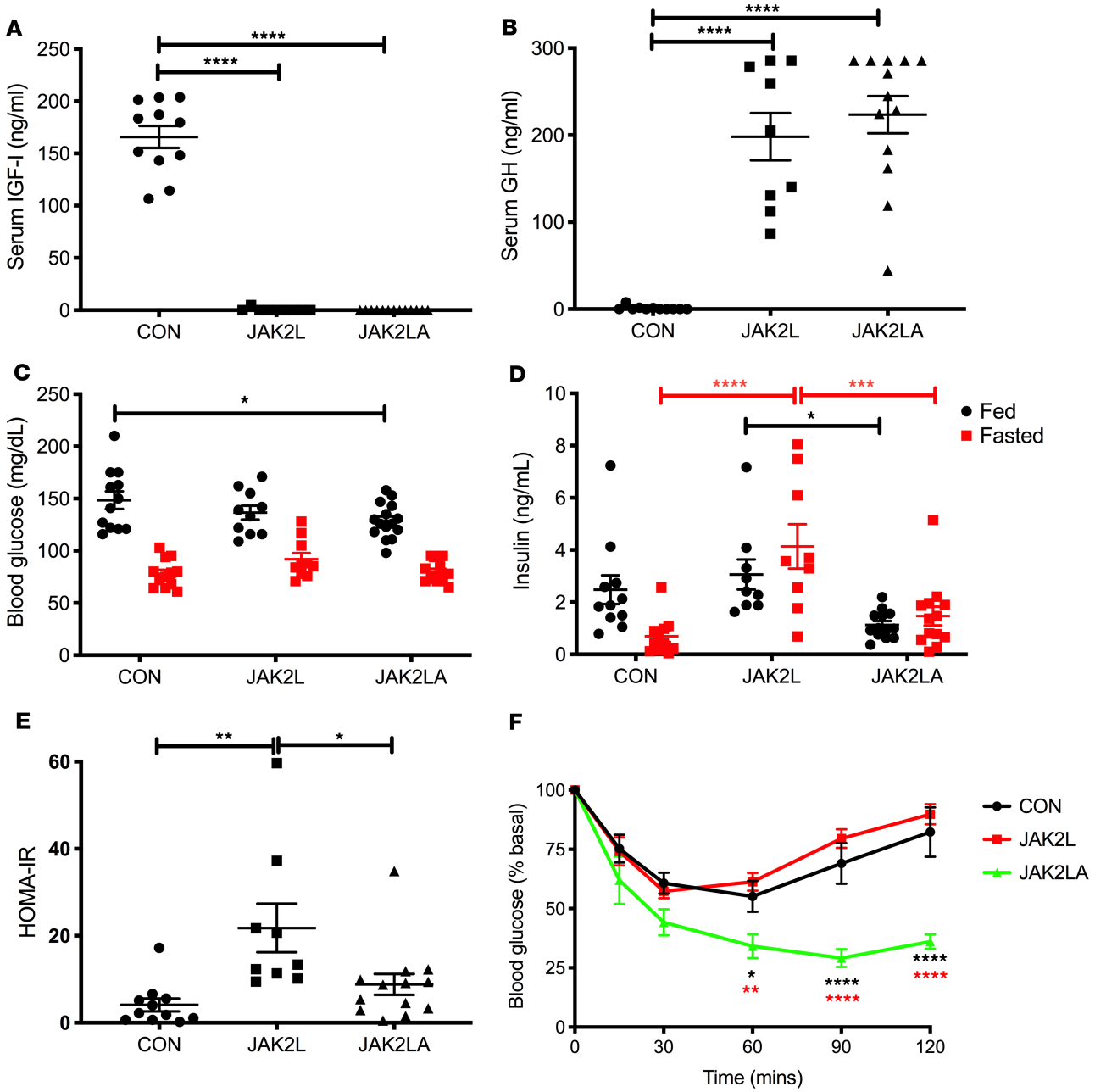

Figure 1. Hepatic GH resistance does not correlate with IR in mice lacking adipocyte *Jak2*. Serum (**A**) IGF1 and (**B**) GH levels in 16-hour-fasted CON, JAK2L, and JAK2LA mice. (**C**) Blood glucose and (**D**) serum insulin levels in ad lib–fed (shown in black) and mice fasted 16 hours (shown in red). (**E**) Homeostatic assessment model of insulin resistance (HOMA-IR) values. (**F**) ITT in CON (black), JAK2L (red), and JAK2LA (green) mice. n = 9–13 (**A**, **B**, **D**, and **E**), 10–15 (**C**), and 6–8 (**F**). $^{*}P < 0.05$; $^{**}P < 0.01$; $^{***}P < 0.001$; $^{****}P < 0.0001$ by 1-way (**A**, **B**, and **E**) and 2-way ANOVA (**C**, **D**, and **F**).

in lean mass and loss of fat mass in JAK2L mice that was normalized in the JAK2LA cohort (Figure 2C). Although relative visceral (epididymal pads) fat mass did not statistically differ among the groups (Figure 2D), a large reduction in subcutaneous (inguinal pads) fat was observed in JAK2L animals, while JAK2LA mice had increased relative subcutaneous fat mass (Figure 2E). Histological sectioning revealed smaller adipocytes and sclerotic tissue in JAK2L inguinal fat pads (Figure 2F). In contrast, JAK2LA fat pads were histologically devoid of fibrotic lesions and contained adipocytes of a size comparable to CON (Figure 2F). At the molecular level, acute refeeding increased levels of phosphorylated (threonine 389) p70S6K, a target of the mammalian target of rapamycin complex 1 (mTORC1) (29), a major regulator of the fasting-to-fed transition (30), in inguinal adipose tissue (Figure 2G). The adipose p70S6K1 response to refeeding was entirely abolished in JAK2L but not JAK2LA mice (Figure 2, G and H). Collectively, high levels of circulating GH

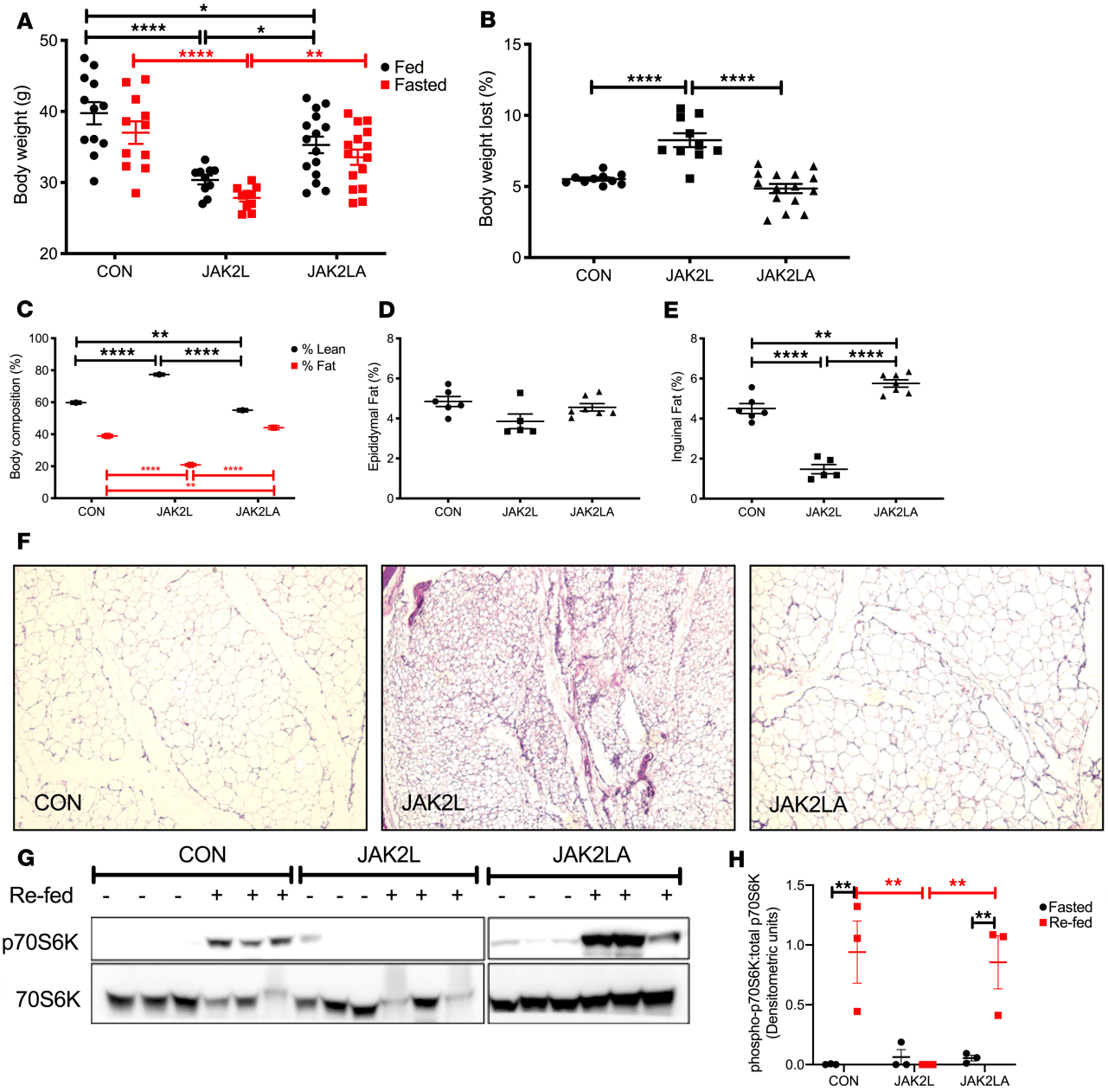

Figure 2. JAK2L mice are lipodystrophic and have a defective fasted-to-fed response in adipose tissue. (**A**) Body weight in grams (g) of ad lib–fed and 16-hour-fasted control CON, JAK2L, and JAK2LA mice. (**B**) Percentage of body weight lost following a 16-hour fast. (**C**) Percentages of lean and fast mass. Amount of (**D**) epididymal and (**E**) inguinal fat mass as a percentage of total body weight. (**F**) H&E staining of inguinal fat pads from 16-hour-fasted mice (original magnification, ×10). (**G**) Inguinal adipose levels (n = 3 per condition) of phosphorylated (T389) p70S6K (top) and total p70S6K (bottom) in 16-hour-fasted (–) or 30-minute-refed (+) mice as determined by Western blot. (**H**) Densitometric quantification of Western blots from (**G**) plotting phosphorylated T389/total p70S6K. n = 10–15 (**A** and **B**), 12–17 (**C**), and 5–7 (**D** and **E**). $^{*}P < 0.05$; $^{**}P < 0.01$; $^{****}P < 0.0001$ by 1-way (**B** and **E**) or 2-way (**A**, **C**, and **H**) ANOVA.

in JAK2L mice were associated with LD and aberrant fasting-to-fed transitional adipose tissue signaling that adipocyte *Jak2* governs.

Loss of hepatocyte Jak2 promotes increased hepatic lipid burden and dyslipidemia in an adipocyte Jak2–dependent manner. Given the association of IR and LD with hepatosteatosis, we examined the livers of aged CON, JAK2L, and JAK2LA mice. As a percentage of total body weight, JAK2L animals had increased liver weight compared with both the CON and JAK2LA cohorts (Figure 3A). In contrast, JAK2LA mice had decreased liver weight (Figure 3A). Both total hepatic triglycerides (Figure 3B) and cholesterol (Figure 3C) were increased in JAK2L mice in an adipocyte *Jak2*–dependent manner. Markers of liver injury, including

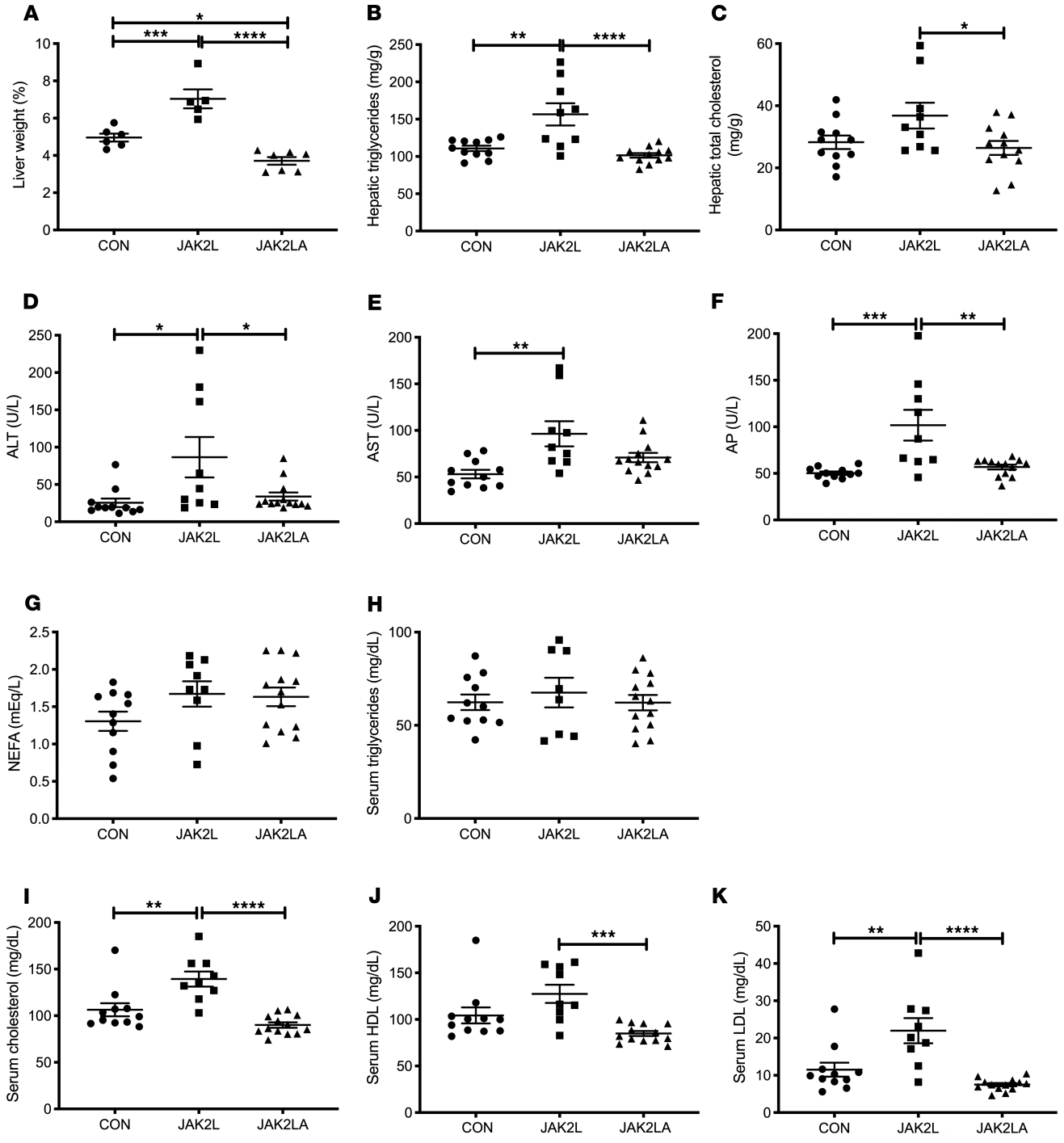

Figure 3. Loss of hepatocyte *Jak2* promotes liver damage and dyslipidemia in an adipocyte *Jak2*–dependent manner. (**A**) Liver weight as a percentage of total body weight in 16-hour-fasted CON, JAK2L, and JAK2LA mice. Hepatic (**B**) triglycerides and (**C**) total cholesterol levels in 16-hour-fasted mice. (**D**) Alanine aminotransferase (ALT), (**E**) aspartate aminotransferase (AST), (**F**) alkaline phosphatase (AP), (**G**) nonesterified fatty acids (NEFAs), (**H**) triglycerides, (**I**) cholesterol, (**J**) high-density lipoprotein (HDL), and (**K**) low-density lipoprotein (LDL) levels in 16-hour-fasted serum. n = 5–7 (**A**), 9–12 (**B** and **C**), and 9–13 (**D**–**K**). *$P < 0.05$; **$P < 0.01$; ***$P < 0.001$; ****$P < 0.0001$ by 1-way ANOVA.

alanine aminotransferase (ALT, Figure 3D), aspartate aminotransferase (AST, Figure 3E), and alkaline phosphatase (AP, Figure 3F) were increased in JAK2L animals, and only AST levels were not entirely normalized in the JAK2LA cohort. Neither fasting serum nonesterified fatty acids (NEFAs, Figure 3G) nor triglycerides (Figure 3H) differed among the groups. However, fasting total cholesterol (Figure 3I) as well as HDL-C (Figure 3J) and LDL-C (Figure 3K) levels were increased in JAK2L mice. Again, these levels were

corrected by concomitant deletion of adipocyte *Jak2*. Thus, hepatic GH resistance promotes increased liver lipid burden, liver injury, and dyslipidemia via effects on adipocytes.

JAK2L mice spontaneously develop age-associated NAFLD and NASH in an adipocyte Jak2–dependent manner. Livers collected from the aged cohorts were sent to a pathologist for a blinded histological assessment. H&E-stained liver sections of aged CON mice demonstrated moderate lipid accumulation, which was slightly increased by hepatocyte-specific deletion of *Jak2* (Figure 4, A–C). In contrast, few lipid droplets were observed in mice with loss of both hepatocyte and adipocyte *Jak2*. Trichrome staining revealed some collagen deposition in the CON cohort, while fibrosis was more widespread in liver sections from JAK2L animals (Figure 4B). Similar to lipid droplets, trichrome staining was reduced in JAK2LA mice. Upon quantification, approximately 54% of CON hepatocytes had lipid droplets, as compared with 74% and 9% for the JAK2L and JAK2LA cohorts, respectively (Figure 4, A and C). For CON and JAK2L livers, steatosis was primarily localized to zone 3, whereas in JAK2LA livers, lipid-laden hepatocytes were also found in the azonal and panacinar regions. Ballooning, an indication of cellular stress, was found to be rare in CON liver sections. In contrast, histological ballooning was much more common in centrizonal sections of JAK2L mice. The severity of ballooning was markedly reduced, but not entirely corrected, by concomitant deletion of adipocyte *Jak2* (Figure 4D). Inflammatory lymphocytic foci were present in about two-thirds of sections examined from CON livers, while foci were identified in all JAK2L sections (Figure 4E). The number of inflammatory foci were reduced in JAK2LA sections as compared with JAK2L but were not completely normalized to CON levels. Scoring for fibrosis (Figure 4F) and Brunt (Figure 4G) staging resulted in highly significant increases for the JAK2L, but not JAK2LA, cohort as compared with CON mice. Thus, JAK2L mice develop NASH with aging with retained JAK2 functioning in adipocytes.

JAK2L mice spontaneously develop HCC. Given that a percentage of patients with NASH develop HCC, we allowed cohorts of CON (n = 17), JAK2L (n = 24), and JAK2LA (n = 20) mice to age until natural death (here, defined as veterinarian-mandated euthanasia). Upon necropsy, livers from both CON and JAK2L were pale and large, while JAK2LA mice had smaller, red-colored livers (Figure 5A). We noticed that a number of livers from JAK2L mice had large growths (Figure 5B). Immunohistochemical assessment of the tumors found them to be fibrotic (Figure 5C) and positive for both glutamine synthetase and glypican-3 (Figure 5D), indicative of HCC (31). Tumor sections were negative for CK19 (Figure 5D), favoring a diagnosis of HCC over cholangiocarcinoma (32). Quantification of HCC incidence in our cohort (Figure 5E) revealed a statistical increase in JAK2L mice (χ^2 test, P = 0.0077), with an average age of discovery of about 704 days. In contrast, HCC incidence in the JAK2LA cohort did not differ from control mice. In summary, mice with high levels of circulating GH due to hepatocyte-specific deletion of *Jak2* spontaneously developed HCC with age. In contrast, high levels of GH in the setting of dual hepatocyte and adipocyte *Jak2* deficiency appear to protect against age-associated HCC.

GH increases hepatic lipid burden through adipocyte Jak2. JAK2 is known to transduce signals from cytokines other than GH. Therefore, the phenotypic changes in hepatic metabolism observed in JAK2L and JAK2LA mice may not be entirely due to loss of GH signaling. To more definitely address the role of GH, we injected CON mice and JAK2A mice with vehicle or GH daily for 7 consecutive days. We chose JAK2A over JAK2LA mice to specifically address the role of adipocyte JAK2, without any confounding effects of combinatorial hepatocyte deletion, in mediating metabolic changes following GH exposure. Livers were collected and subjected to a liquid chromatography-mass spectrometry panel targeting approximately 200 lipids. Heatmaps derived from the top 99% of lipid species detected show that GH treatment grossly augmented hepatic TAG (Figure 6A) and DAG (Figure 6B; for raw lipidomics data and concentration waterfall plots, see Supplemental Table 1 and Supplemental Figure 1, respectively; supplemental material available online with this article; https://doi.org/10.1172/jci.insight.131310DS1) species in CON mice. One week of GH treatment increased total hepatic TAG (Figure 6C) and DAG (Figure 6D) by an average of approximately 18% and 15%, respectively, in CON but not JAK2A mice. Hepatic cholesterol ester (CE) species were less affected by GH treatment (Figure 6E). However, GH treatment in CON mice did produce statistically higher levels of total hepatic CE than in JAK2A animals (Figure 6G). GH treatment did not differentially affect total hepatic ceramide (CER) when comparing CON and JAK2A cohorts (Figure 6, F and H). Therefore, acute GH treatment increases hepatic lipid burden but does so via adipocyte signaling.

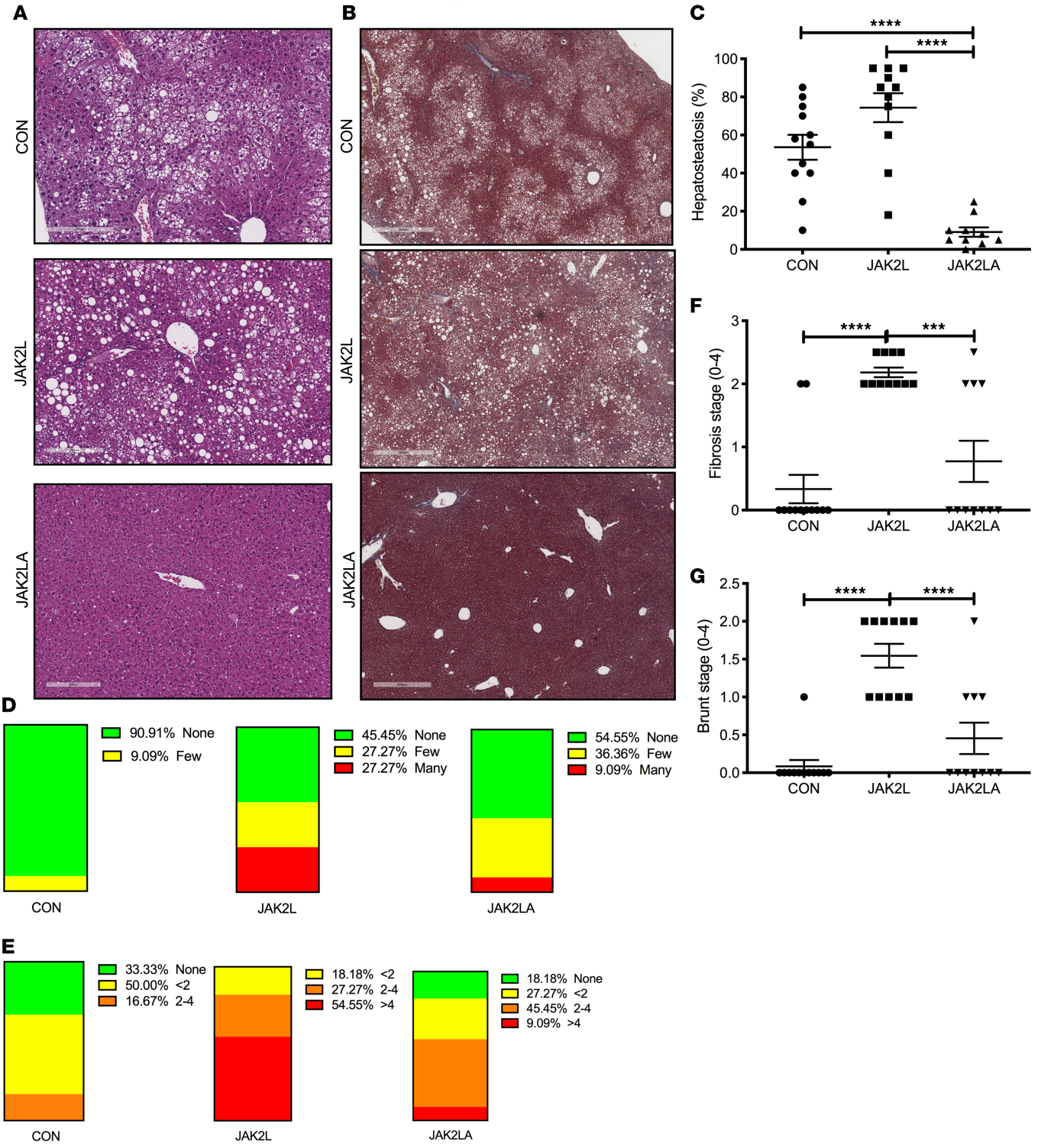

Figure 4. Loss of hepatocyte *Jak2* promotes NAFLD and NASH in an adipocyte *Jak2*–dependent manner. (**A**) H&E and (**B**) trichrome staining of liver sections from CON, JAK2L, and JAK2LA mice. (**C**) Percentages of hepatosteatosis, (**D**) ballooning, and (**E**) inflammatory loci observed in liver sections. (**F**) Fibrosis staging score. (**G**) Brunt staging score. n = 10–12. ***$P < 0.001$; ****$P < 0.0001$ by 1-way ANOVA.

Discussion

The association between IR and type 2 diabetes (T2D) with hepatosteatosis is strong (33). However, it presents a number of physiological quandaries. Chief among them is why fatty liver develops in the setting of IR (34). The normal physiological roles of insulin action on the liver are to suppress hepatic glucose production

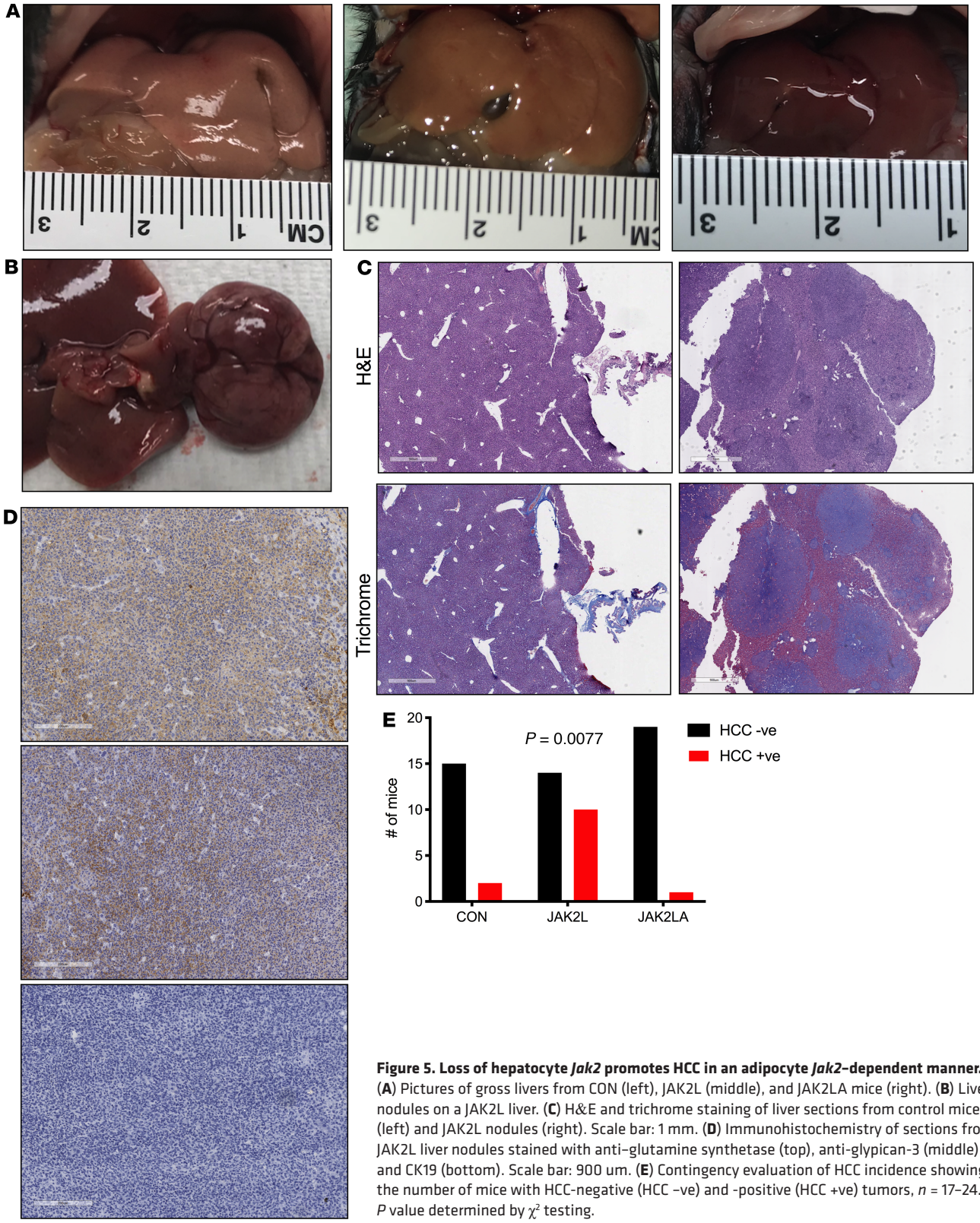

Figure 5. Loss of hepatocyte *Jak2* promotes HCC in an adipocyte *Jak2*–dependent manner. (**A**) Pictures of gross livers from CON (left), JAK2L (middle), and JAK2LA mice (right). (**B**) Liver nodules on a JAK2L liver. (**C**) H&E and trichrome staining of liver sections from control mice (left) and JAK2L nodules (right). Scale bar: 1 mm. (**D**) Immunohistochemistry of sections from JAK2L liver nodules stained with anti–glutamine synthetase (top), anti-glypican-3 (middle), and CK19 (bottom). Scale bar: 900 um. (**E**) Contingency evaluation of HCC incidence showing the number of mice with HCC-negative (HCC –ve) and -positive (HCC +ve) tumors, n = 17–24. P value determined by χ^2 testing.

(HGP) and to stimulate TAG synthesis. Thus, the prediction would be that patients with T2D would have hyperglycemia (from the inability of insulin to suppress HGP) concomitant with "normal" liver lipid levels (from the inability of insulin to induce TAG synthesis). Nevertheless, patients with T2D, while indeed exhibiting increased gluconeogenesis, also display increased rates of TAG synthesis, suggesting the latter pathway

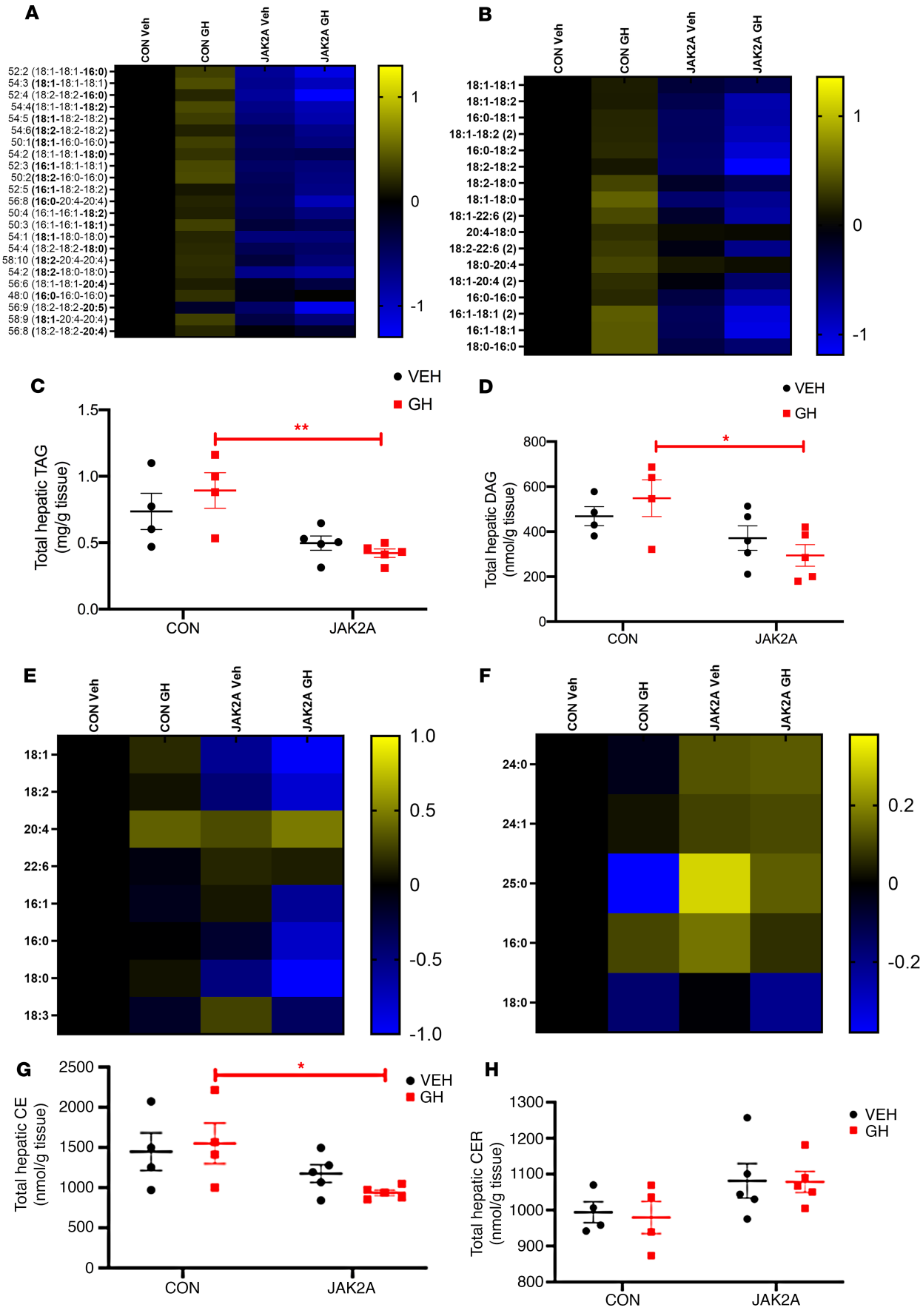
A
CON Veh
CON GH
JAK2A Veh
JAK2A GH
52:2 (18:1-18:1-16:0)
54:3 (18:1-18:1-18:1)
52:4 (18:2-18:2-16:0)
54:4(18:1-18:1-18:2)
54:5 (18:1-18:2-18:2)
54:6(18:2-18:2-18:2)
50:1(18:1-16:0-16:0)
54:2 (18:1-18:1-18:0)
52:3 (16:1-18:1-18:1)
50:2(18:2-16:0-16:0)
52:5 (16:1-18:2-18:2)
56:8 (16:0-20:4-20:4)
50:4 (16:1-16:1-18:2)
50:3 (16:1-16:1-18:1)
54:1 (18:1-18:0-18:0)
54:4 (18:2-18:2-18:0)
58:10 (18:2-20:4-20:4)
54:2 (18:2-18:0-18:0)
56:6 (18:1-18:1-20:4)
48:0 (16:0-16:0-16:0)
56:9 (18:2-18:2-20:5)
58:9 (18:1-20:4-20:4)
56:8 (18:2-18:2-20:4)
1
0
-1
B
CON Veh
CON GH
JAK2A Veh
JAK2A GH
18:1-18:1
18:1-18:2
16:0-18:1
18:1-18:2 (2)
16:0-18:2
18:2-18:2
18:2-18:0
18:1-18:0
18:1-22:6 (2)
20:4-18:0
18:2-22:6 (2)
18:0-20:4
18:1-20:4 (2)
16:0-16:0
16:1-18:1 (2)
16:1-18:1
18:0-16:0
1
0
-1
C
VEH
GH
Total hepatic TAG (mg/g tissue)
1.5
1.0
0.5
0.0
**
CON
JAK2A
D
VEH
GH
Total hepatic DAG (nmol/g tissue)
800
600
400
200
0
*
CON
JAK2A
E
CON Veh
CON GH
JAK2A Veh
JAK2A GH
18:1
18:2
20:4
22:6
16:1
16:0
18:0
18:3
1.0
0.5
0
-0.5
-1.0
F
CON Veh
CON GH
JAK2A Veh
JAK2A GH
24:0
24:1
25:0
16:0
18:0
0.2
0
-0.2
G
Total hepatic CE (nmol/g tissue)
2500
2000
1500
1000
500
0
*
VEH
GH
CON
JAK2A
H
Total hepatic CER (nmol/g tissue)
1300
1200
1100
1000
900
800
VEH
GH
CON
JAK2A

Figure 6. GH treatment induces hepatic lipid deposition via adipocyte *Jak2*. Lipidomics heatmaps of individual hepatic (**A**) triacylglycerol (TAG), (**B**) diacylglycerol (DAG), (**E**) cholesterol ester (CE), and (**F**) ceramide (CER) species in vehicle-treated (Veh-treated) or GH-treated CON and JAK2A mice. Total hepatic (**C**) TAG, (**D**) DAG, (**G**) CE, and (**H**) CER levels. $^{*}P < 0.05$; $^{**}P < 0.01$ by 2-way ANOVA. For lipidomics heatmaps, all values of individual lipid species are expressed as the $\log_2$ ratio to Veh-treated CON mice and visualized by the $\log_2$ scale to the right of the heatmap. n = 4–5.

remains active while the former loses insulin responsiveness. This paradox has been termed "selective hepatic IR" and has been primarily attributed to branch points (i.e., 1 arm regulating HGP and a second mediating TAG synthesis) of insulin signaling within the liver itself (10, 11). TAG synthesis via hepatic DNL has been proposed as the potential driver of fatty liver disease (35) and a target of hepatic GH action (25). The natural conclusion would be to treat T2D and metabolic liver disease by targeting liver-intrinsic mechanisms.

An alternative hypothesis is that substrate delivery can drive HGP and TAG synthesis independent of direct effects of insulin on the liver (36). From this vantage, diseases associated with hepatic IR could be treated by either shutting off the supply of substrate or inhibiting substrate uptake. In support of this, a study on patients with NAFLD demonstrated that the majority of hepatic TAG arises from NEFAs, more than twice of that derived from DNL (37). Furthermore, it was reported in high fat diet–fed rats that NEFA but not hepatic TAG accumulation is the cause of liver cell injury (38). Regardless, registered interventional NASH trials almost exclusively examine the effects of agents targeting mechanisms within the liver. Therefore, the effects of abrogating substrate supply or uptake remain unexamined, although preclinical models are supportive of pursuing this paradigm (38, 39). Here, we show that inhibition of adipocyte JAK2 signaling prevents the sequelae of events associated with high levels of circulating GH, beginning with IR and progressing through HCC. Specifically, the potential, if any, of inhibiting adipocyte GH signaling for the treatment of established NAFLD, NASH, and HCC is unknown.

Short-term starvation is a natural state of IR and fatty liver (40). During nutrient deprivation, GH induces IR and promotes a lipolytic response (15). It has been hypothesized that GH resistance, which results in high circulating GH levels, is an adaptive response to states of undernutrition to maintain euglycemia (41). Adipocyte (42) but not hepatocyte (43) IR results in LD and can promote fatty liver. This suggests that starvation and LD-induced fatty liver may share a common mechanism involving GH-mediated adipocyte IR. Interestingly, although AN is characterized by GH resistance (i.e., elevated circulating GH in the face of low plasma IGF1), treatment of AN patients with GH further induces fat loss. This suggests that AN is actually a state of *hepatic* GH resistance while adipose tissue of patients with AN remains GH responsive. Consistent with this, we now show that mice with elevated GH (JAK2L) lose more body weight following a 16-hour fast and are lipodystrophic. We interpret this as an unrestrained chronic state of adipose tissue IR and a condition mimicking metabolic starvation. At the molecular level, adipose tissue of JAK2L mice failed to induce mTORC1 following acute refeeding, suggesting that GH impinges on mTORC1 activity. Interestingly, loss of mTORC1 specifically in adipocytes induces IR, fatty liver disease, and LD (44), a phenocopy of the JAK2L mice. These phenotypes associated with loss of hepatocyte *Jak2* — IR, attenuation of adipose tissue mTORC1 activation, LD, and fatty liver — are rescued in JAK2LA mice. Therefore, adipocytes govern GH-mediated catabolism and fat mobilization and subsequent perturbation of liver metabolism.

Adult GH deficiency (AGHD) commonly results in the development of NAFLD and NASH (24). The association of AGHD with fatty liver has been attributed to the ability of GH to inhibit hepatic DNL; hence, in the absence of liver GH action, DNL would be increased (25). This is in contrast with our previous work using in vivo ^2H_2O labeling because we found no increase in DNL in mice with fatty liver lacking hepatic GH signaling (26). Instead, using precise, tissue-specific genetic models, we have determined that fatty acid uptake, via Cd36, is responsible for liver-intrinsic mechanisms driving fatty liver in mice with disrupted hepatic GH signaling (39). Further, hepatosteatosis following hepatic GH resistance is dependent on circulating GH, and because GH cannot transduce hepatic signals in the setting of hepatic GH resistance, a tissue other than liver must mediate fatty liver development (26). Here, our lipidomics data demonstrate that 1 week of GH treatment promoted lipid deposition in livers of mice with intact hepatic GH signaling but not in mice lacking adipocyte GH signaling. Thus, both loss of hepatic GH sensitivity as well as continued hepatic exposure to GH in GH-sensitive animals promotes fatty liver. This may seem contradictory except that hepatic GH resistance results in high levels of circulating GH, similar to peripheral administration of recombinant GH. As we show here, hepatosteatosis induced by either GH resistance or GH treatment is governed by adipocyte JAK2. Regardless, the association of AGHD with liver fat and dysfunction has led to the dominant paradigm of augmenting GH levels to treat NAFLD and NASH. We propose that this

approach will likely worsen the pathophysiology of established NAFLD and NASH, as was reported for patients with AN (18) and HIV-associated LD (45, 46).

Cordoba-Chacon et al. recently reported that knockdown of hepatocyte *Ghr* in adult mice (aHepGHRkd) promotes fatty liver and NASH via increased DNL without severe alterations in systemic metabolism or adipose tissue lipolysis (47). This led them to conclude that liver disease from loss of hepatocyte GH signaling occurs via liver-autonomous means. However, it is difficult to make these conclusions in the face of high circulating GH, as reported in their aHepGHRkd mice, which can act on non-liver tissue, as well as IR (hyperinsulinemia and hyperglycemia). Previously, we controlled for augmented circulating GH in mice lacking hepatocyte GH signaling by global disruption of GH secretion (26). These studies demonstrated that circulating GH mediated onset of fatty liver in JAK2L mice, demonstrating that cells other than hepatocytes were responsible for development of hepatosteatosis. aHepGHRkd did not display increased plasma NEFAs, which is consistent with our study here because we did not observe a correlation between circulating fasting NEFA levels and liver pathology. However, given that circulating NEFA levels are the net result of release and uptake, and that loss of hepatic GH signaling induces *Cd36* (which increases NEFA uptake), it is difficult to make any conclusions on the state of lipolysis (39). To directly address this, Cordoba-Chacon et al. (47) used adipose explant cultures to demonstrate that aHepGHRkd had normal basal and stimulated rates of lipolysis. This is also consistent with our previously published results showing that GH does not affect basal lipolysis but instead specifically interferes with the ability of insulin to suppress lipolysis (19). Thus, without directly attending to high circulating GH levels present in aHepGHRkd mice via concomitant loss of adipocyte *Ghr* or global *Gh* disruption, it is premature to conclude that fatty liver and NASH resulting from loss of hepatocyte *Ghr* occurs via liver-autonomous means.

The role of JAK2/STAT5 signaling in HCC is well documented. Liver-specific *Stat5* knockouts (STAT5L), like our JAK2L mice here, succumb to HCC on aging without carcinogen or dietary intervention (48). In a study by Yu, Zhu, Riedlinger, Kang, and Hennighausen, STAT5L mice developed HCC at age 17 months, although it was a small cohort of 4 mice. In addition, a previous study examined liver tumorigenesis in JAK2L mice and reported a 68% incidence at 60 weeks of age, although it is unclear whether the tumors were HCC (49). Here, we report that 10/24 (~42%) of JAK2L mice developed HCC with an average age of discovery of about 704 days. Contrary to these findings, 1 report found that loss of hepatocyte *Jak2* protects against liver tumorigenesis (50). However, the work by Shi et al. used chemical and dietary perturbations to induce liver disease and carcinogenesis. We propose that findings from the reports, including our own, on aging-related HCC are mediated by adipocyte GH signaling and governed by IR while orally administered carcinogens and dietary models directly affect hepatocytes. Our work here demonstrates that JAK2L mice succumb specifically to the sequelae of events leading to metabolic liver disease and, although it is experimentally cumbersome to wait approximately 2 years for HCC development, may provide a more faithful model of human IR-associated HCC.

Acromegaly predisposes to cancer, and cancer has become a leading cause of acromegaly-associated deaths, despite an overall increase in life expectancy due to new treatments (51). The most parsimonious rationale for the mechanism of cancer onset due to high levels of GH is increased plasma IGF1. However, we report here that mice with hepatic GH resistance indeed succumb to HCC, despite undetectable circulating IGF1. Further, while treatment of Laron syndrome (LS) patients (loss of GH signaling) with recombinant IGF1 does normalize linear growth rates, restoration of IGF1 levels by pharmacological means does not prevent the immunity from cancer appreciated in those with LS (52). Collectively, then, we propose that GH predisposes to cancer via its role in metabolism and not IGF1 production, possibly through actions on adipose tissue. Adipose tissue dysfunction, and IR in particular, is highly associated with cancer and adipocytes have been proposed as mediators of tumor cell behavior (53). How insulin-resistant adipocytes promote oncogenesis is unknown, but a role for fatty acid receptors has been proposed (54). In addition, metabolic reprogramming in HCC is mediated by the master oncogene *Myc* (55), and MYC levels themselves are induced by cellular exposure to fatty acids (56). Interestingly, a single bolus of GH increased hepatic *Myc* expression within 1 hour of administration (57). Therefore, it is tempting to speculate that adipocytes release a factor in a JAK2-dependent manner that subsequently induces hepatic *Myc*, leading to a favorable metabolic environment for development of HCC. Given that HCCs are "addicted" to sustained MYC expression (58), it will be interesting to test whether inhibition of adipocyte JAK2 will lead to regression of established HCC, what would ultimately be akin to a kind of "metabolite addiction."

Our current study excluded female mice. This is particularly relevant to NAFLD and NASH because sexual dimorphism is a characteristic of the disease (59). Females are relatively protected from metabolic dysregulation in both humans and mice, and this has been attributed to, among other sex-based differences, a preferential partitioning of FA toward ketogenesis over VLDL TAG production (60). Our studies here were a follow-up to previous work using hyperinsulinemic-euglycemic clamps (19, 20), where the high degree of variability between female animals when using this technique presented a resource-based limitation for us. Therefore, females were not included in the current aging study because we have yet to definitely determine the state of insulin sensitivity in either JAK2L or JAK2LA female mice. Regardless, this is a major limitation in our report that we hope to remediate in the future.

Methods

Animals and diets. The generation of JAK2L and JAK2LA mice using *Albumin:Cre* and *Adiponectin:Cre* was previously described (20). For our studies reported here, *Jak2*$^{lox/lox}$ (61) were used as controls and backcrossed onto the C57BL/6 background for at least 9 generations. We used male mice only in these studies, and all animals were maintained on PicoLab Mouse Diet 20 (Lab Diet 5058; percentage of calories provided by protein, 23%; fat, 22%; and carbohydrate, 55%) throughout their lifetime.

Study designs. Mice were aged until 70 to 75 weeks for metabolic studies. Blood was collected by retro-orbital puncture at 1700 hours before food removal as the fed state. The following morning at 0900 hours, mice were sacrificed and blood and tissues collected as the fasted state. For refeeding studies, mice fasted overnight were sacrificed or refed for 30 minutes before tissue collection by placing a pellet of food into the cages. Tissues were flash frozen on liquid nitrogen for Western blot, lipidomics, and transcriptomic analyses. Tissues were fixed with 10% neutral-buffered formalin for 24 hours for histological analyses. Blood glucose and serum insulin levels were determined by glucometer readings (Bayer Contour) and ELISA (Alpco), respectively. Serum IGF1 (R&D MG100) and GH (MilliporeSigma EZRMGH-45K) levels were determined by ELISA. For ITT, mice were fasted for 4 hours (0900–1300 hours) followed by i.p. injection of 2 U/kg insulin (Novolin Novo Nordisk). Blood glucose levels were determined by tail prick using a handheld glucometer at the times indicated. HOMA-IR was calculated as a ratio of fasting blood glucose (mg/dL) to fasting serum insulin (mU/L) divided by 405 (62). Total fat mass was determined by dual-energy x-ray absorptiometry. All clinical chemistry was done on terminally collected serum from mice fasted 16 hours and done at the University of California, Davis, Comparative Pathology Lab Core. For acute GH studies, CON and JAK2A mice were injected (i.p.) with vehicle (0.03 M $NaHCO_3$ and 0.15 M NaCl, pH 9.5) or 5 mg/kg recombinant mouse GH (AF Parlow, National Hormone and Peptide Program, UCLA) daily at 0900 hours for 7 days and sacrificed 4 hours after a fast and the final injection.

Hepatic TAG and cholesterol measurements and Western blots. Bits of frozen liver were weighed and resuspended in 1× cell lysis buffer (Cell Signaling Technology 9803) with protease (Roche 4693132001) and phosphatase (Roche 4906845001) inhibitor cocktail at a final volume of 50 mg/mL and homogenized using the OmniTH homogenizer. Twenty microliters of lysates was used to determine cholesterol (Wako 999-02601) and triglyceride (Infinity reagent, Thermo Fisher Scientific TR22421) levels. Alternatively, lysates were run out on 4% to 12% gradient gels and probed with anti–p(T389) p70S6K (Cell Signaling 9205) and anti-p70S6K (Cell Signaling 2708) antibodies. Western blots were developed with SuperSignal West Femto reagent (Thermo Fisher Scientific 34095) and developed using a ChemiDoc Imaging System (Bio-Rad). Densitometric quantification was carried out using ImageJ (NIH) software as described previously (63).

Liver histology and pathological analyses. Tissues were collected and fixed in 10% neutral-buffered formalin for 24 hours. Subsequently, tissues were washed and stored in 70% ethanol until embedding and sectioning. Sectioning and staining were carried out by the UCSF Liver Center core. H&E, trichrome, reticulin, and immunohistochemical stains were reviewed and evaluated by a blinded gastrointestinal/liver pathologist. Livers were evaluated and scored according to methods by Kleiner and Brunt (64). Liver tumors were evaluated by H&E, trichrome, and reticulin patterns and further evaluated by immunohistochemical staining for CK19, glutamine synthetase, and glypican-3. Immunohistochemical staining was performed by Peninsula Laboratories International.

Lipidomics. Lipidomics were done exactly as described previously (20).

Statistics. All statistical tests and figures were done using GraphPad Prism v8.0. The type of ANOVA test (1 or 2 way) and resulting *P* values are indicated in the figure legends. *P* values of less than 0.05 were considered significant. All scatter dot plots shown are plotted as the mean ± SEM.

Study approval. All procedures performed on animals were in accordance with regulations and established guidelines and were reviewed and approved by the Institutional Animal Care and Use Committee at the UCSF.

Author contributions

JLT and KCC carried out experiments for Figures 1–5. JLT and CGW did the ITTs for Figure 1. JLT and DL performed experiments for Figure 6. ANM did all liver pathological analyses. NBV and MC performed lipidomics, made heatmap and waterfall plots, and provided Supplemental Table 1. KCC carried out all ELISAs and Western blot analyses. KCC and EJW conceived of the experiments, made the figures, performed statistical analyses, and wrote the paper.

Acknowledgments

This study was supported by NIH grants 1R01DK091276 (to EJW) and DK076169 (to EJW). We also gratefully acknowledge the support of the James Peter Read Foundation, the UCSF Cardiovascular Research Institute, the UCSF Diabetes Center (P30 DK063720), the UCSF Liver Center (P30 DK026743), and the National Institute of Diabetes and Digestive and Kidney Diseases (NIDDK) (K08DK098270, to ARN). We would like to thank Kay-Uwe Wagner from the University of Nebraska for providing the *Jak2* conditional mice.

Address correspondence to: Ethan J. Weiss, 555 Mission Bay Blvd. S., Room 382Y, UCSF, San Francisco, California, USA 94158. Phone: 415.514.0819; Email: ethan.weiss@ucsf.edu. Or to: Aras N. Mattis, 513 Parnassus Ave., Room HSW-516, UCSF, San Francisco, California, USA 94141. Phone: 415.514.3062; Email: aras.mattis@ucsf.edu.

1. Younossi Z, et al. Global burden of NAFLD and NASH: trends, predictions, risk factors and prevention. *Nat Rev Gastroenterol Hepatol*. 2018;15(1):11–20.
2. Kanwal F, et al. Risk of hepatocellular cancer in patients with non-alcoholic fatty liver disease. *Gastroenterology*. 2018;155(6):1828–1837.e2.
3. Ghouri YA, Mian I, Rowe JH. Review of hepatocellular carcinoma: epidemiology, etiology, and carcinogenesis. *J Carcinog*. 2017;16:1.
4. Hansen HH, Feigh M, Veidal SS, Rigbolt KT, Vrang N, Fosgerau K. Mouse models of nonalcoholic steatohepatitis in preclinical drug development. *Drug Discov Today*. 2017;22(11):1707–1718.
5. Van Herck MA, Vonghia L, Francque SM. Animal models of nonalcoholic fatty liver disease — a starter's guide. *Nutrients*. 2017;9(10):E1072.
6. Marchesini G, et al. Association of nonalcoholic fatty liver disease with insulin resistance. *Am J Med*. 1999;107(5):450–455.
7. Marchesini G, et al. Nonalcoholic fatty liver disease: a feature of the metabolic syndrome. *Diabetes*. 2001;50(8):1844–1850.
8. Mancina RM, et al. Paradoxical dissociation between hepatic fat content and de novo lipogenesis due to PNPLA3 sequence variant. *J Clin Endocrinol Metab*. 2015;100(5):E821–E825.
9. Geisler CE, Renquist BJ. Hepatic lipid accumulation: cause and consequence of dysregulated glucoregulatory hormones. *J Endocrinol*. 2017;234(1):R1–R21.
10. Brown MS, Goldstein JL. Selective versus total insulin resistance: a pathogenic paradox. *Cell Metab*. 2008;7(2):95–96.
11. Ferris HA, Kahn CR. Unraveling the paradox of selective insulin resistance in the liver: the brain-liver connection. *Diabetes*. 2016;65(6):1481–1483.
12. Moller L, Stodkilde-Jorgensen H, Jensen FT, Jorgensen JO. Fasting in healthy subjects is associated with intrahepatic accumulation of lipids as assessed by 1H-magnetic resonance spectroscopy. *Clin Sci*. 2008;114(8):547–552.
13. Melvin A, O'Rahilly S, Savage DB. Genetic syndromes of severe insulin resistance. *Curr Opin Genet Dev*. 2018;50:60–67.
14. Duval C, et al. Adipose tissue dysfunction signals progression of hepatic steatosis towards nonalcoholic steatohepatitis in C57BL/6 mice. *Diabetes*. 2010;59(12):3181–3191.
15. Sakharova AA, et al. Role of growth hormone in regulating lipolysis, proteolysis, and hepatic glucose production during fasting. *J Clin Endocrinol Metab*. 2008;93(7):2755–2759.
16. Gahete MD, Córdoba-Chacón J, Luque RM, Kineman RD. The rise in growth hormone during starvation does not serve to maintain glucose levels or lean mass but is required for appropriate adipose tissue response in female mice. *Endocrinology*. 2013;154(1):263–269.
17. Tzagournis M, George J, Herrold J. Increased growth hormone in partial and total lipoatrophy. *Diabetes*. 1973;22(5):388–396.
18. Fazeli PK, et al. Effects of recombinant human growth hormone in anorexia nervosa: a randomized, placebo-controlled study. *J Clin Endocrinol Metab*. 2010;95(11):4889–4897.
19. Corbit KC, et al. Adipocyte JAK2 mediates growth hormone-induced hepatic insulin resistance. *JCI Insight*. 2017;2(3):e91001.
20. Corbit KC, et al. Adipocyte JAK2 regulates hepatic insulin sensitivity independently of body composition, liver lipid content, and hepatic insulin signaling. *Diabetes*. 2018;67(2):208–221.
21. Guevara-Aguirre J, et al. Growth hormone receptor deficiency is associated with a major reduction in pro-aging signaling, cancer,

and diabetes in humans. *Sci Transl Med*. 2011;3(70):70ra13.
22. Guevara-Aguirre J, Procel P, Guevara C, Guevara-Aguirre M, Rosado V, Teran E. Despite higher body fat content, Ecuadorian subjects with Laron syndrome have less insulin resistance and lower incidence of diabetes than their relatives. *Growth Horm IGF Res*. 2016;28:76–78.
23. Olarescu NC, Bollerslev J. The impact of adipose tissue on insulin resistance in acromegaly. *Trends Endocrinol Metab*. 2016;27(4):226–237.
24. Takahashi Y. The role of growth hormone and insulin-like growth factor-I in the liver. *Int J Mol Sci*. 2017;18(7):E1447.
25. Cordoba-Chacon J, et al. Growth hormone inhibits hepatic de novo lipogenesis in adult mice. *Diabetes*. 2015;64(9):3093–3103.
26. Sos BC, et al. Abrogation of growth hormone secretion rescues fatty liver in mice with hepatocyte-specific deletion of JAK2. *J Clin Invest*. 2011;121(4):1412–1423.
27. Nordstrom SM, Tran JL, Sos BC, Wagner KU, Weiss EJ. Disruption of JAK2 in adipocytes impairs lipolysis and improves fatty liver in mice with elevated GH. *Mol Endocrinol*. 2013;27(8):1333–1342.
28. Tripathy D, Almgren P, Tuomi T, Groop L. Contribution of insulin-stimulated glucose uptake and basal hepatic insulin sensitivity to surrogate measures of insulin sensitivity. *Diabetes Care*. 2004;27(9):2204–2210.
29. Saitoh M, Pullen N, Brennan P, Cantrell D, Dennis PB, Thomas G. Regulation of an activated S6 kinase 1 variant reveals a novel mammalian target of rapamycin phosphorylation site. *J Biol Chem*. 2002;277(22):20104–20112.
30. Laplante M, Sabatini DM. mTOR signaling in growth control and disease. *Cell*. 2012;149(2):274–293.
31. Wasfy RE, Shams Eldeen AA. Roles of combined glypican-3 and glutamine synthetase in differential diagnosis of hepatocellular lesions. *Asian Pac J Cancer Prev*. 2015;16(11):4769–4775.
32. Tao LY, Cai L, He XD, Liu W, Qu Q. Comparison of serum tumor markers for intrahepatic cholangiocarcinoma and hepatocellular carcinoma. *Am Surg*. 2010;76(11):1210–1213.
33. Gaggini M, Morelli M, Buzzigoli E, DeFronzo RA, Bugianesi E, Gastaldelli A. Non-alcoholic fatty liver disease (NAFLD) and its connection with insulin resistance, dyslipidemia, atherosclerosis and coronary heart disease. *Nutrients*. 2013;5(5):1544–1560.
34. Brown MS, Goldstein JL. Selective versus total insulin resistance: a pathogenic paradox. *Cell Metab*. 2008;7(2):95–96.
35. Lally JSV, et al. Inhibition of acetyl-CoA carboxylase by phosphorylation or the inhibitor ND-654 suppresses lipogenesis and hepatocellular carcinoma. *Cell Metab*. 2019;29(1):174–182.e5.
36. Vatner DF, et al. Insulin-independent regulation of hepatic triglyceride synthesis by fatty acids. *Proc Natl Acad Sci U S A*. 2015;112(4):1143–1148.
37. Donnelly KL, Smith CI, Schwarzenberg SJ, Jessurun J, Boldt MD, Parks EJ. Sources of fatty acids stored in liver and secreted via lipoproteins in patients with nonalcoholic fatty liver disease. *J Clin Invest*. 2005;115(5):1343–1351.
38. Liu J, Han L, Zhu L, Yu Y. Free fatty acids, not triglycerides, are associated with non-alcoholic liver injury progression in high fat diet induced obese rats. *Lipids Health Dis*. 2016;15:27.
39. Wilson CG, Tran JL, Erion DM, Vera NB, Febbraio M, Weiss EJ. Hepatocyte-specific disruption of CD36 attenuates fatty liver and improves insulin sensitivity in HFD-fed mice. *Endocrinology*. 2016;157(2):570–585.
40. Lundbaek K. Metabolic abnormalities in starvation diabetes. *Yale J Biol Med*. 1948;20(6):533–544.
41. Fazeli PK, Klibanski A. Determinants of GH resistance in malnutrition. *J Endocrinol*. 2014;220(3):R57–R65.
42. Qiang G, et al. Lipodystrophy and severe metabolic dysfunction in mice with adipose tissue-specific insulin receptor ablation. *Mol Metab*. 2016;5(7):480–490.
43. Michael MD, et al. Loss of insulin signaling in hepatocytes leads to severe insulin resistance and progressive hepatic dysfunction. *Mol Cell*. 2000;6(1):87–97.
44. Lee PL, Tang Y, Li H, Guertin DA. Raptor/mTORC1 loss in adipocytes causes progressive lipodystrophy and fatty liver disease. *Mol Metab*. 2016;5(6):422–432.
45. Lo J, et al. Low-dose physiological growth hormone in patients with HIV and abdominal fat accumulation: a randomized controlled trial. *JAMA*. 2008;300(5):509–519.
46. Schwarz JM, et al. Effects of recombinant human growth hormone on hepatic lipid and carbohydrate metabolism in HIV-infected patients with fat accumulation. *J Clin Endocrinol Metab*. 2002;87(2):942.
47. Cordoba-Chacon J, Sarmento-Cabral A, Del Rio-Moreno M, Diaz-Ruiz A, Subbaiah PV, Kineman RD. Adult-onset hepatocyte GH resistance promotes NASH in male mice, without severe systemic metabolic dysfunction. *Endocrinology*. 2018;159(11):3761–3774.
48. Yu JH, Zhu BM, Riedlinger G, Kang K, Hennighausen L. The liver-specific tumor suppressor STAT5 controls expression of the reactive oxygen species-generating enzyme NOX4 and the proapoptotic proteins PUMA and BIM in mice. *Hepatology*. 2012;56(6):2375–2386.
49. Themanns M, et al. Hepatic deletion of Janus kinase 2 counteracts oxidative stress in mice. *Sci Rep*. 2016;6:34719.
50. Shi SY, et al. Janus Kinase 2 (JAK2) dissociates hepatosteatosis from hepatocellular carcinoma in mice. *J Biol Chem*. 2017;292(9):3789–3799.
51. Bolfi F, Neves AF, Boguszewski CL, Nunes-Nogueira VS. Mortality in acromegaly decreased in the last decade: a systematic review and meta-analysis. *Eur J Endocrinol*. 2018;179(1):59–71.
52. Laron Z, Kauli R. Fifty seven years of follow-up of the Israeli cohort of Laron Syndrome patients — from discovery to treatment. *Growth Horm IGF Res*. 2016;28:53–56.
53. Duong MN, Geneste A, Fallone F, Li X, Dumontet C, Muller C. The fat and the bad: mature adipocytes, key actors in tumor progression and resistance. *Oncotarget*. 2017;8(34):57622–57641.
54. Suckow AT, Briscoe CP. Key questions for translation of FFA receptors: from pharmacology to medicines. *Handb Exp Pharmacol*. 2017;236:101–131.
55. Camarda R, Williams J, Goga A. In vivo reprogramming of cancer metabolism by MYC. *Front Cell Dev Biol*. 2017;5:35.
56. Artwohl M, et al. Different mechanisms of saturated versus polyunsaturated FFA-induced apoptosis in human endothelial cells. *J Lipid Res*. 2008;49(12):2627–2640.
57. Murphy LJ, Bell GI, Friesen HG. Growth hormone stimulates sequential induction of c-myc and insulin-like growth factor I expression in vivo. *Endocrinology*. 1987;120(5):1806–1812.

58. Shachaf CM, et al. MYC inactivation uncovers pluripotent differentiation and tumour dormancy in hepatocellular cancer. *Nature*. 2004;431(7012):1112–1117.
59. Ballestri S, Nascimbeni F, Baldelli E, Marrazzo A, Romagnoli D, Lonardo A. NAFLD as a sexual dimorphic disease: role of gender and reproductive status in the development and progression of nonalcoholic fatty liver disease and inherent cardiovascular risk. *Adv Ther*. 2017;34(6):1291–1326.
60. Marinou K, Adiels M, Hodson L, Frayn KN, Karpe F, Fielding BA. Young women partition fatty acids towards ketone body production rather than VLDL-TAG synthesis, compared with young men. *Br J Nutr*. 2011;105(6):857–865.
61. Krempler A, Qi Y, Triplett AA, Zhu J, Rui H, Wagner KU. Generation of a conditional knockout allele for the *Janus kinase 2* (*Jak2*) gene in mice. *Genesis*. 2004;40(1):52–57.
62. Yokoyama H, et al. Quantitative insulin sensitivity check index and the reciprocal index of homeostasis model assessment in normal range weight and moderately obese type 2 diabetic patients. *Diabetes Care*. 2003;26(8):2426–2432.
63. Davarinejad H. Quantifications of Western Blots with ImageJ. York University Web Site. http://www.yorku.ca/yisheng/Internal/Protocols/ImageJ.pdf. Accessed August 21, 2019.
64. Kleiner DE, Brunt EM. Nonalcoholic fatty liver disease: pathologic patterns and biopsy evaluation in clinical research. *Semin Liver Dis*. 2012;32(1):3–13.